THE JOURNAL OF PHYSICAL CHEMISTRY C
A JOURNAL OF THE AMERICAN CHEMICAL SOCIETY

pubs.acs.org/JPCC
Article

Computational Modeling of Hydrated Polyamine-Based Anion Exchange Membranes via Molecular Dynamics Simulation

Eleonora Tomasino, Binayak Mukherjee, Varun Donnakatte Neelalochana, Paolo Scardi, and Narges Ataollahi*

Cite This: J. Phys. Chem. C 2024, 128, 623−634

ABSTRACT: The present study aims to investigate static and dynamic properties of polyamine-based anion exchange membranes (AEMs) using all-atom molecular dynamics simulations. The effects of the hydration level, degree of amination, and temperature on the properties of AEMs were systematically explored. The phase segregation and the formation of interconnected hydrophilic channels were visualized for different simulated membranes. Additionally, the variation of the diffusion coefficients of both water molecules and hydroxide anions as a function of the aforementioned parameters were computed, and the mechanical properties of the different membranes were studied. The results revealed that increasing the degree of amination and water uptake facilitates the transport of water and anionic species. However, this comes at the expense of the mechanical stability of the membrane due to water-induced plasticization, potentially leading to its irreversible deformation under operating conditions. We then demonstrate that a promising compromise solution between high conductivity and mechanical stability can be achieved by limiting the degree of amination to about 30%. These results furnish valuable insights into the development of improved AEMs.

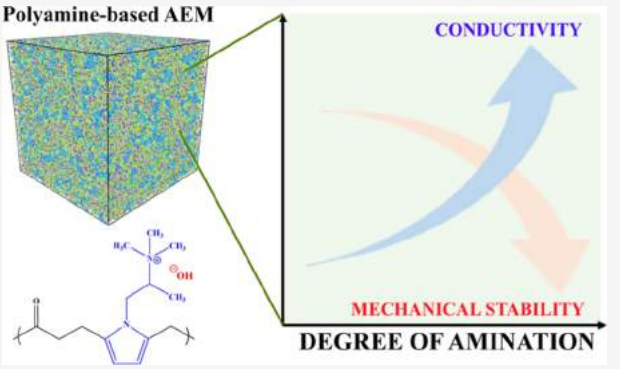

INTRODUCTION

In recent years, there has been growing interest in anion exchange membranes (AEMs) in the field of energy conversion and storage. AEMs are used for fuel cells and water electrolyzers, with potential for utilization in other applications, such as storage systems, redox flow batteries, and water desalination.[1−9] Although their ionic conductivity is not comparable yet to that of proton exchange membranes (PEMs),[10] AEMs are appealing alternatives due to their improved kinetics for the oxygen reduction reaction, the absence of precious metal catalyst, the lower costs, and the minimization of corrosion problems in alkaline environment.[11−13]

AEMs contain positively charged functional groups that facilitate the passage of anions from the cathode to the anode in the membrane−electrode assembly.[14] These functional groups are generally quaternary ammonium (QA) ions, although alternative cationic groups are being investigated.[15−19] Among the AEMs with QA head groups, polyamine (PA)-based AEMs have been synthesized by the modification of polyketone via Paal−Knorr condensation reaction.[1,3,5,20−26] These membranes are functionalized by trimethylammonium quaternary groups via a methylation reaction, followed by an OH-exchange process (Scheme 1).

Scheme 1. Functionalized PA Single Monomer, with Trimethylammonium Head Group and a Pyrrolic Ring in the Backbone

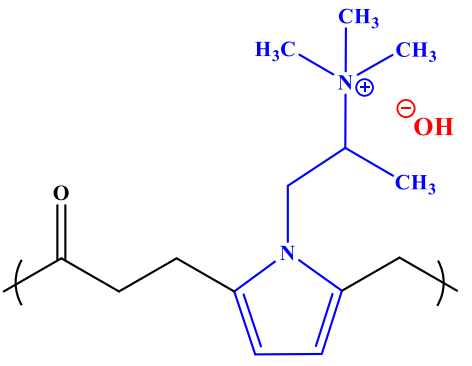

Received: October 27, 2023
Revised: December 7, 2023
Accepted: December 11, 2023
Published: December 21, 2023

https://doi.org/10.1021/acs.jpcc.3c07118
J. Phys. Chem. C 2024, 128, 623−634

Table 1. Details on the Structure and Composition of Simulated Membranes

membrane	degree of amination (%)	λ	OH^- ions	H_2O molecules	total atoms	single-cell size [nm]
membrane 1	10	6	60	300	9600	4.49
membrane 2	10	9	60	480	10,140	4.56
membrane 3	10	12	60	660	10,690	4.64
membrane 4	10	15	60	840	11,220	4.72
membrane 5	30	6	180	900	15,480	5.19
membrane 6	30	9	180	1440	17,100	5.39
membrane 7	30	12	180	1980	18,720	5.61
membrane 8	30	15	180	2520	20,340	5.73
membrane 9	50	6	300	1500	21,360	5.77
membrane 10	50	9	300	2400	24,060	6.01
membrane 11	50	12	300	3300	26,760	6.24
membrane 12	50	15	300	4200	29,460	6.46

The interest in PA membranes mainly relies on the use of inexpensive and easily modifiable polyketone as a starting material to tailor the properties of the final polymer. Moreover, PA membranes have high dimensional stability and can withstand temperatures up to 200 °C,[1] despite displaying lower conductivity compared to PEMs.[1,3,22,24,26]

Computational modeling has proven to be a powerful tool to unfold both static and dynamic properties of polymer membranes.[27] Classical molecular dynamics (MD) simulations have been widely conducted to provide a better understating and insights into the different properties of PEMs and AEMs.[28] For instance, Rezayani et al.[10,29] performed atomistic-level MD simulations on poly(2,6-dimethyl-1,4-phenylene oxide) with QA pendant chains (PPO−QA). They investigated the role of the hydrated morphology and the pendant cationic groups in ion diffusion in AEMs. Kuo et al.[30] analyzed the morphology of hydrated perfluorosulfonic acid (PFSA) membranes with increasing water content, using all-atom MD simulation on large simulation boxes. Di Salvo et al.[31] applied ab initio density functional theory (DFT) analysis and MD simulations to analyze the effect of ion exchange capacity (IEC) on water uptake and ionic transport in polysulfone−tetramethylammonium membranes. Zhang et al.[32] used MD simulation to understand the correlation between poly(arylpiperidinium) backbone and the performance of the AEM, in terms of ionic conductivity and swelling resistance. Feng et al.[33] investigated the mechanical behavior of hydrated PFSA membranes for PEMFCs. Finally, Dong et al.[34−36] used combined reactive and nonreactive polarizable force fields to estimate the contribution of Grotthuss and vehicular diffusion mechanisms in AEMs.

PA has been previously analyzed by means of ab initio DFT[37] to investigate the impact of the different monomer regions on water uptake, ionic transport, and degradation mechanism. The results pointed out the significance of QA groups in water cluster formation and conductivity, while the carbonyl groups, though hydrophilic, do not participate in the diffusion of hydroxide species. On the other hand, the hydrophobic backbone permits the nanophase segregation of the membrane and the repulsion of the ions into the water channels.

The properties of the membranes are closely related to the chemistry of the polymer and the morphology under hydrated conditions. The development of an interconnected water network is a critical factor for water and ion transport through the system.[10]

In this study, all-atom MD simulations were used to investigate various features of the membranes, including nanophase segregation, transport, and mechanical properties, under the influence of hydration level, degree of amination, and temperature.

To date, most of the studies have been conducted using small simulation boxes (<10 nm side), due to the difficulties and high computational costs encountered by simulating large cells.[30] In this work, we examined the effect of system size on the different simulations and found that larger cells (∼20 nm cubic box length) are required for mechanical properties, while smaller systems (∼6 nm) are sufficient for transport properties and morphology analysis.

This study provides a starting point for an optimized design of AEMs, aimed at an overall improvement in the performance of the electrochemical device.

COMPUTATIONAL METHOD

Simulation Details. In this study, we simulated a variety of PA membranes with different degrees of amination (10, 30, and 50%). The percentage represents the number of functional groups present in the polymer chain. The structure of the single ionized PA monomer was initially optimized by running ab initio calculations based on DFT.[37]

Random copolymer chains were obtained alternating ionized and nonionized monomers. Each chain has a degree of polymerization equal to 20, with 2, 6, and 10 QA groups, respectively. All QA groups are supposed to be fully ionized, while no neutral amine groups are present. To grant electroneutrality, one OH^- ion per QA group was added to the system.

All simulation cells contain 30 polymer chains and the corresponding number of hydroxide anions based on the degree of amination. Four hydration levels are investigated (λ = 6, 9, 12, 15), where λ is defined as the number of water molecules and hydroxide anions per cationic group. The details of the simulated structures are listed in Table 1.

The initial cubic boxes with periodic boundary conditions were generated using the Amorphous Builder tool of Materials Studio MedeA software.[38] The polymer chains, hydroxide anions, and water molecules were randomly arranged in a cell with an initial low density (0.2 g/mL) to avoid any problem of ring concatenation and polymer entanglements.[39]

All-atom MD simulations were carried out using the large-scale atomic/molecular massively parallel simulator (LAMMPS).[40] The pcff+ force field[41,42] was employed for both polymer and solvent molecules, and the individual atomic charges assigned by the chosen force-field were adopted. The equations of motion were integrated using the velocity Verlet

https://doi.org/10.1021/acs.jpcc.3c07118
J. Phys. Chem. C 2024, 128, 623−634

algorithm.[43] The long-range Coulombic interactions were computed via the particle−particle/particle−mesh method[44] with an accuracy of 0.00001. The van der Waals interactions were described via the 6/9 Lennard-Jones potential[45] with a cutoff distance of 1.0 nm. The temperature and the pressure of the systems were controlled using the Nose−Hoover thermostat and barostat[46] for the canonical ensemble (*NVT*) and the isothermal−isobaric ensemble (*NPT*).[47]

An initial energy minimization was performed, followed by an *NPT* relaxation at $T = 293$, $P = 1$ atm, and a time step of 1.0 fs. The minimization was executed for 1 ns to gradually compress the cell to a density approaching the experimental value (~1.1 g/cm^3). Equilibration was reached through an annealing process from 293 to 600 K, with temperature steps of 100 K, via alternating *NVT* and *NPT* ensembles. The procedure was repeated three times, to confirm that the density had attained a constant value.[30,47] This operation was required to fully relax any residual stress that might be introduced during the construction of the model. An additional 100 ns of *NPT* ensemble at 300 K and 1 atm were conducted to achieve further equilibration.[30] The relaxed structures were used for subsequent dynamic analysis, calculating diffusion coefficients, and Young's moduli at different temperatures (from 293 to 393 K).

Three cells of varying dimensions were analyzed to determine the effect of the system size on the properties. The medium (2 × 2 × 2) and large (3 × 3 × 3) simulation boxes were generated by replicating the structure of a single cell. Additional details on the density, size, and number of atoms for each cell are provided in Table S1.

Simulation Analysis. *Morphology, Radial Distribution Function, and Coordination Number.* The radial distribution functions (RDF) and the coordination numbers (CN) of selected atom pairs were obtained with LAMMPS. The RDF $g_{A\to B}(r)$ indicates the local probability density of finding atoms B at a distance r from atoms A, averaged over the equilibrium trajectory, as expressed by eq 1

$$g_{A\to B}(r) = \left(\frac{n_B}{4\pi r^2 \Delta r}\right)/\left(\frac{N_B}{V}\right) \tag{1}$$

The CN denotes the total number of neighbors of a reference particle within a certain distance r, and can be calculated as[48]

$$CN = \int_0^{r'} \frac{N_B}{V} 4\pi r^2 g(r)\, dr \tag{2}$$

The N−O_{OH} RDF provides information on the solvation of the cationic group by OH^- ions; the O_{OH}−O_W RDF defines the solvation of the anionic species by water molecules (O_w); the O_w−O_w RDF probes the formation of water clusters and can be used to investigate the internal structure of water phase; finally, the N−N RDF enables quantification of the swelling of the membrane upon water uptake or temperature increase. In addition, the CN of the O_{OH}−O_W couple were analyzed to quantify the number of water molecules presents in the solvation shell of the anionic species; the N−N CN provides information on the overlapping of the hydration shells of neighboring side chains; and the N−O_{OH} CN suggests the sharing of hydroxide anions between two different cationic groups.

Potential Mean Force. The potential mean force (PMF) is a powerful tool to quantify the strength of the interaction between the hydroxide anion and the QA group in terms of the free energy of dissociation. It is calculated from the N−O_{OH} RDF, according to the eq 4[49]

$$PMF = -RT \ln(g(r)) \tag{3}$$

where R is the gas constant, T is the temperature, and $g(r)$ is the N−O_{OH} RDF.

Diffusion Coefficient. The water and hydroxide diffusion in AEMs occurs by means of two main mechanisms, namely vehicular diffusion and hopping (Grotthuss) mechanisms.[50−56] Vehicular diffusion is a physical process that is driven by pressure and potential gradients. The Grotthuss mechanism, instead, is a chemical process that involves the continuous formation and breaking of hydrogen bonds between OH^- and the water molecules. In the present work, the pcff+ force field was employed to qualitatively probe the vehicular diffusion only, which constitutes a fraction of the overall ionic conductivity.[30,31] A reactive force field is more suitable for studying processes involving chemical reactions.[36,48,57,58] However, at present, we think that a qualitative analysis is enough for the scope of this review, which is to prove the opposite trends of ionic conductivity and mechanical stability of the membrane. Overall, a similar trend is expected, even though Grotthuss mechanism is significantly enhancing ion diffusivity, as proved by other works.[34−36,57]

The self-diffusion coefficients of hydroxide anions and water molecules are calculated following the mean square displacement (MSD) route.[10,29,59]

$$MSD(t) = \langle |r_j(t) - r_j(0)|^2 \rangle = 2dDt \tag{4}$$

where r is the position of the particle j at time t or 0, D is the diffusion coefficient, and d is the topological dimension, equal to 3 in the case of three-dimensional diffusion.

The MSD curves were computed using LAMMPS software, and the self-diffusion coefficients were derived from the long-time linear slope of the MSD curve, according to Einstein's relation

$$D = \frac{\langle |r_j(t) - r_j(0)|^2 \rangle}{6t} \tag{5}$$

The above equations apply to uniform normal diffusion in a 3D Brownian motion.

However, in polymeric systems, the Fickian regime is often not achieved, especially at lower temperatures and hydration levels. This can be attributed to various phenomena, such as side chain hindrance, electrostatic interactions between anions and cationic groups, and confinement at the nanoscale.[10,29,60]

In these cases, it would be more correct to employ the generalized form of Einstein's relation, which introduces a time- and length-scale-dependent anomalous diffusion coefficient (D_a) and an anomalous diffusion exponent (n), given by the slope of the logarithmic plot of the MSD

$$MSD(t) = \langle |r_j(t) - r_j(0)|^2 \rangle = 2dD_a t^n \tag{6}$$

$$n(t) = \frac{d\ln\langle \Delta r^2(t) \rangle}{d \ln t} \tag{7}$$

A value of $n < 1$ is an index of a subdiffusive regime. Whereas as n approaches 1 the normal (Fickian) diffusion regime could be assumed. The values of anomalous diffusion exponents were calculated to quantify the deviation from normal diffusion.

https://doi.org/10.1021/acs.jpcc.3c07118
J. Phys. Chem. C 2024, 128, 623−634

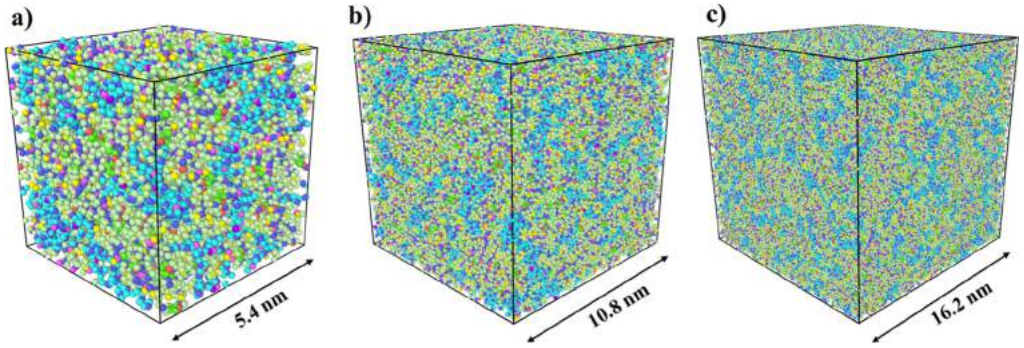

Figure 1. Membrane 6 with three different sizes: (a) single cell, (b) 2 × 2 × 2 supercell, and (c) 3 × 3 × 3 supercell, with dimensions of 5.4, 10.8, and 16.2 nm, respectively.

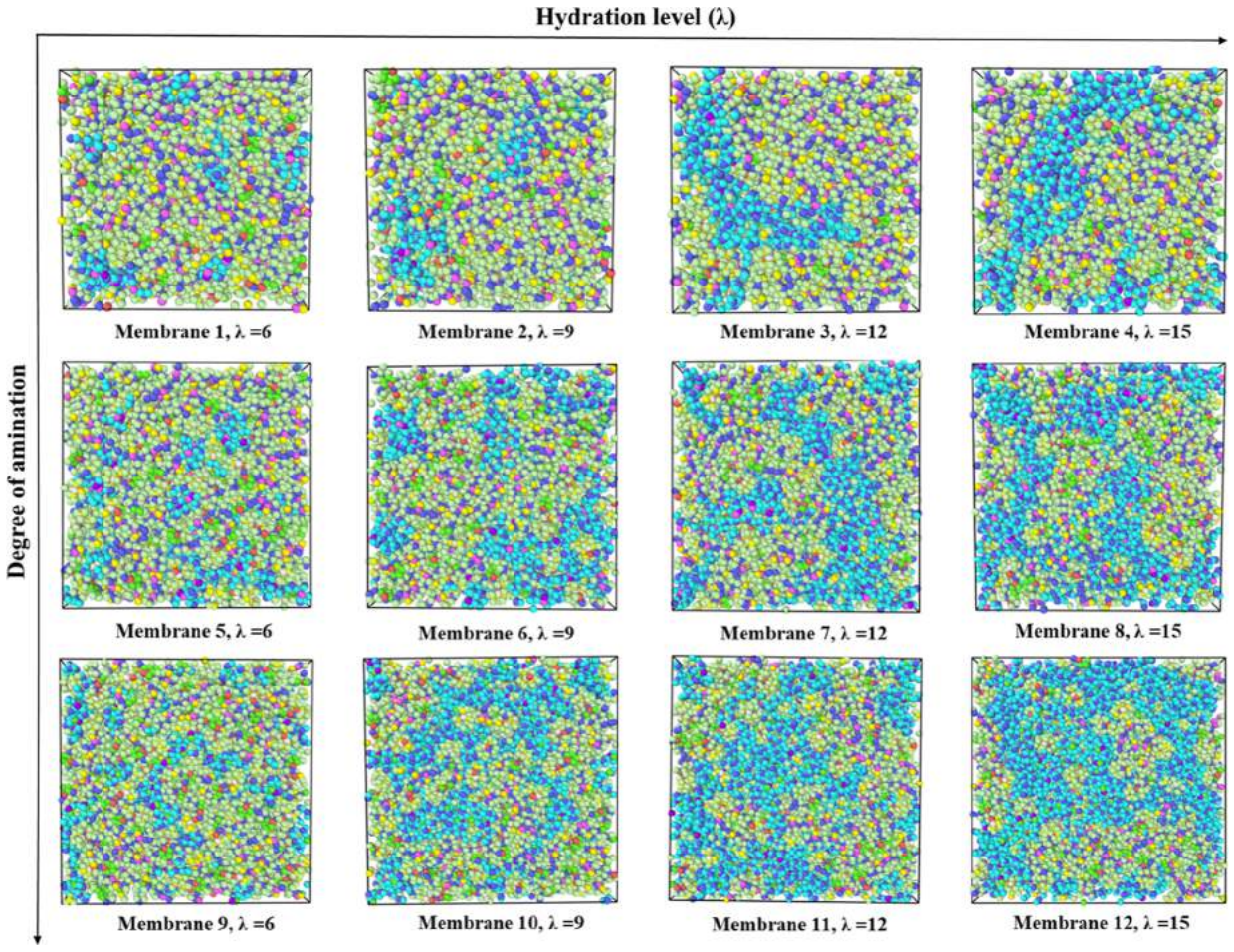

Figure 2. Nanophase segregation of membranes varying the degree of amination and the water content λ.

Mechanical Deformation. Investigating the structural integrity of hydrated membranes under different operating conditions is crucial, as they are susceptible to many physical and chemical degradation mechanisms.[33,61,62] The mechanical properties are closely related to the hydration level, temperature, strain rate, and polymer chemistry. MD simulation at the atomic level is a valuable technique for determining the impact of these parameters on fundamental properties, such as the elastic modulus, yield stress, and yield strain. However, due to the use of necessarily short length and time scales and a fast strain rate typical of MD, results cannot be directly compared with experimental values as they relate with very small representative volume elements far from the mesoscopic scale. Nevertheless, MD outcomes preserve a somewhat general qualitative validity at a smaller length scale.

The simulations were conducted on 3 × 3 × 3 supercells applying a constant engineering strain rate of 10^{-7}/fs in the x direction. Zero pressure was maintained in the other directions to allow for box striction. The tensile axial deformation was applied for 3 ns. An *NPT* ensemble with a Nose−Hoover thermostat was used to keep a constant temperature during deformation. For the simulations at different temperatures, alternating *NPT* and *NVT* ensembles were executed prior to strain application to reach the desired temperature and further relax the structure.

https://doi.org/10.1021/acs.jpcc.3c07118
J. Phys. Chem. C 2024, 128, 623−634

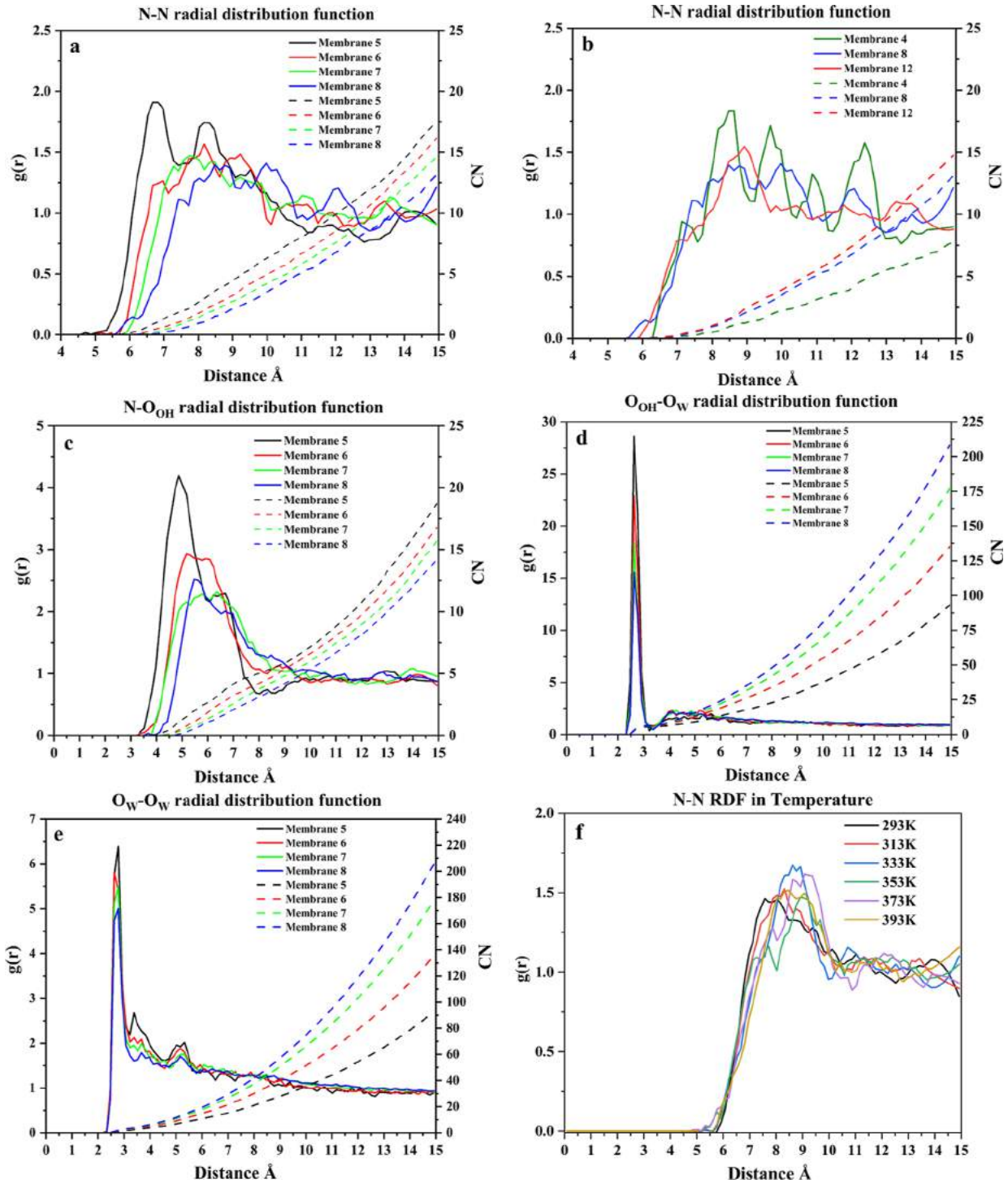

Figure 3. N−N (a), N−O_{OH} (c), O_{OH}−O_W (d), and O_W−O_W (e) RDFs and CN (dashed lines) of membranes with 30% of amination and variable water content; (b) N−N RDF and CN of membranes with λ = 15; and (f) N−N RDF of membrane 7 with variable temperature (refer to Table 1 for membranes specifications).

Size Effect Analysis. The effect of the system size was investigated before conducting the different simulations. While size has no influence on the morphology of membranes,[30] an examination was carried out for the dynamic properties.

Membrane 6 (having the average parameters) was selected for simulations with three different cell dimensions. The starting geometry was a single cell with a side length of 5.4 nm. The larger cells, 2 × 2 × 2 and 3 × 3 × 3 supercells, have dimensions of 10.8 and 16.2 nm, respectively (Figure 1).

Diffusion and mechanical tests were performed on the three systems, and the results are shown in the Supporting Information. No significant changes were observed in diffusion coefficients, but system size strongly affected mechanical properties. Increasing the dimension of the simulation cell reduced the boundary effects and allowed for the use of a lower strain rate (10^{-7}/fs instead of 10^{-9}/fs used for the single cell), approaching the order of magnitude of experimental Young's moduli (Figure S1).

https://doi.org/10.1021/acs.jpcc.3c07118
J. Phys. Chem. C 2024, 128, 623−634

In conclusion, simulations of the static and transport properties were carried out using a single cell system to reduce the computational costs. Conversely, the mechanical properties were simulated using the larger (3 × 3 × 3) cells, to ensure more accurate results.

RESULTS AND DISCUSSION

Validation of the Simulations. The final structures of the fully relaxed systems were validated by comparing the simulated density to experimental data. The experimentally measured density for hydrated membranes at room temperature ranged between 1.10 and 1.20 g/cm^3, while dry membrane has a density of 1.11 g/cm^3. In comparison, the computed densities after annealing processes and 100 ns *NPT* simulations ranged between 1.08 and 1.11, and 1.08 g/cm^3 in dry conditions, in good agreement with experimental results.

The equilibrium densities for the systems at various hydration levels are reported in Table S1 and Figure S2. Regardless of the degree of amination, all simulated membranes exhibited a decrease in density as the water content increased. This behavior is explained by the formation of larger water clusters and channels that expand the membrane and reduce the average density of the simulated system. The only exception was the system with a 10% amination. An increase in density was observed as λ shifted from 6 to 9, due to the initial filling of the void spaces formed within the material. The addition of water after the voids are filled leads to the weakening of interchain interactions causing membrane swelling.[63] This trend is consistent with other simulations reported in the literature.[49,64] A further validation of the force field used was provided by a comparison of RDF results with DFT and reactive force field analyses, as discussed in the following sections.

Morphology of Hydrated Membranes. Figure 2 shows the simulation boxes after a full relaxation, showing the nanoscale morphology of the water clusters and channels formed inside the membranes upon water uptake. At low hydration levels (λ = 6), small and isolated water clusters are dispersed throughout the membrane. By increasing water content, the hydrophilic network becomes more and more interconnected, forming a hydrophilic pathway for ionic transport. Particularly, membranes with 10% of amination exhibited a developed water network only at λ = 15, indicating that the diffusion of water molecules and anionic species does not occur at lower water content. In contrast, the hydrophilic network is already formed at lower values of λ for the membranes with 30 and 50% of amination.

RDF and CN. The results of the N−N RDF of membranes with 30% amination and varying water content are displayed in Figure 3a.

Two peaks, at 6.7 and 8.2 Å, are visible at the lowest value of λ (membrane 5). As water content increases, the peaks weaken and merge into a single peak, shifting toward higher distances (from 6.7 to 8.7 Å at λ = 15), indicating a progressive increase in the distance between the QA groups. This effect can be attributed to membrane swelling upon water uptake, consistently with the literature.[10] The same behavior was observed for membranes with 10 and 50% amination (Figures S3a and S4a).

Figure 3b shows the CN trends of the N−N couple for all membranes with λ = 15. Correspondingly to the first peak, membranes with 30 and 50% amination both exhibit CN ∼ 2, while CN ∼ 1 is observed for the membrane with 10% amination. In the second case, the distance between the amine groups is greater and the hydration shells of neighboring side chains are not overlapping, which could be the reason for the much lower diffusivity. In fact, Chen et al.[64] demonstrated that these overlapping regions constitute the preferential pathway for anionic conductivity.

The N−O_{OH} $g(r)$ is shown in Figure 3c. The stronger peak at 4.9 Å in membrane 5 suggests that hydroxide ions are positioned near the QA head groups, consistent with the results from ab initio simulations.[37] As the hydration level increases, the peak weakens and shifts over longer distances. This is attributed to the solvation effect of water molecules, which reduces the electrostatic interaction with the cationic group. At higher degrees of amination (Figures S3b and S4b), the significant lowering of the peak intensity is a clue for a weaker N−O interaction. In all cases, a second weak peak (a shoulder) was observed at ca. 6.5 Å, corresponding to a second hydration shell of the cationic group. The N−O_{OH} CN in correspondence with the second peak is ∼2, further demonstrating the overlapping of the solvation shells of neighboring side chains.[49] Figure 3d displays the O_{OH}−O_W RDF. All membranes exhibit a distinct peak at approximately 2.6 Å, which decreases in intensity as the water content rises. This peak is attributed to the first hydration shell of water molecules surrounding the OH^-, and the reduction in the intensity is due to the solvation effect of H_2O. A second weaker peak, attributed to the second hydration shell of the ionic species, was observed at 4 Å. A CN of 4.5 is always present in the first hydration shell. The lower value of CN in correspondence with the second peak for λ = 6 indicates that the second hydration shell is not well developed in this case.

O_W−O_W $g(r)$ of the O_W−O_W and CN are shown in Figure 3e. The sharp peak at 2.7 Å and the weaker peak at ∼5.2 Å represent the first and second hydration shells of water molecules, respectively. The increasing CN at higher λ suggests the formation of larger water clusters.

Additionally, the thermal expansion of membrane 7 was investigated by determining the N−N RDF at varying temperatures (from 293 to 393 K), as shown in Figure 3f. As the temperature increases, the main peak shifts from ∼7.8 to ∼9.0 Å, indicating a thermal expansion of the membrane. However, the effect of temperature is not as significant as that of water uptake. This could be assigned to the thermal stability of the membrane, as proved by experimental measurements.[47]

The RDF results were utilized to validate the pcff+ force field parameters. The main peaks of the O_{OH}−O_W, O_W−O_W, and N−O_{OH} of membrane 5 were compared to the distances resulting from quantum chemical calculations of a single PA monomer. The structure, interacting with one OH^- and five water molecules (λ = 6), was subjected to geometry minimization. DFT analysis was carried out with ORCA software[65] using Becke-3-parameter−Lee−Yang−Parr (B3LYP) functional and 6-311G** basis set. The charge-dependent atom-pairwise dispersion correction (D4) by Grimme[66] was used to include dispersion forces. The results (Table S2) prove the effectiveness of the pcff+ force field.

A final validation was carried out using a reactive force field. The ReaxFF parameters were taken from Zhang et al.,[36] which have been developed for the analysis of hydrated AEMs. The previously optimized cells have been prepared for the transition to ReaxFF following the procedure developed by Pisani et al.[67] To avoid cell explosion at high temperatures, the

https://doi.org/10.1021/acs.jpcc.3c07118
J. Phys. Chem. C 2024, 128, 623−634

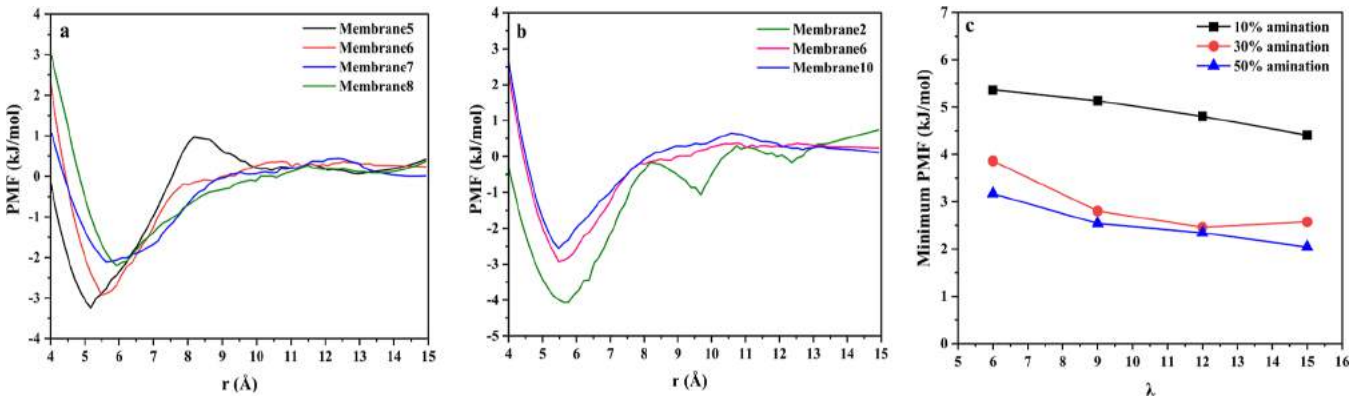

Figure 4. PMF of (a) membranes with 30% of amination and variable hydration level λ and (b) membranes with λ = 9 and variable degree of amination; and (c) minimum (absolute) values of PMF for membranes with 10 (black), 30 (red), and 50% (blue) of amination, as a function of the level of hydration λ (refer to Table 1 for membranes specifications).

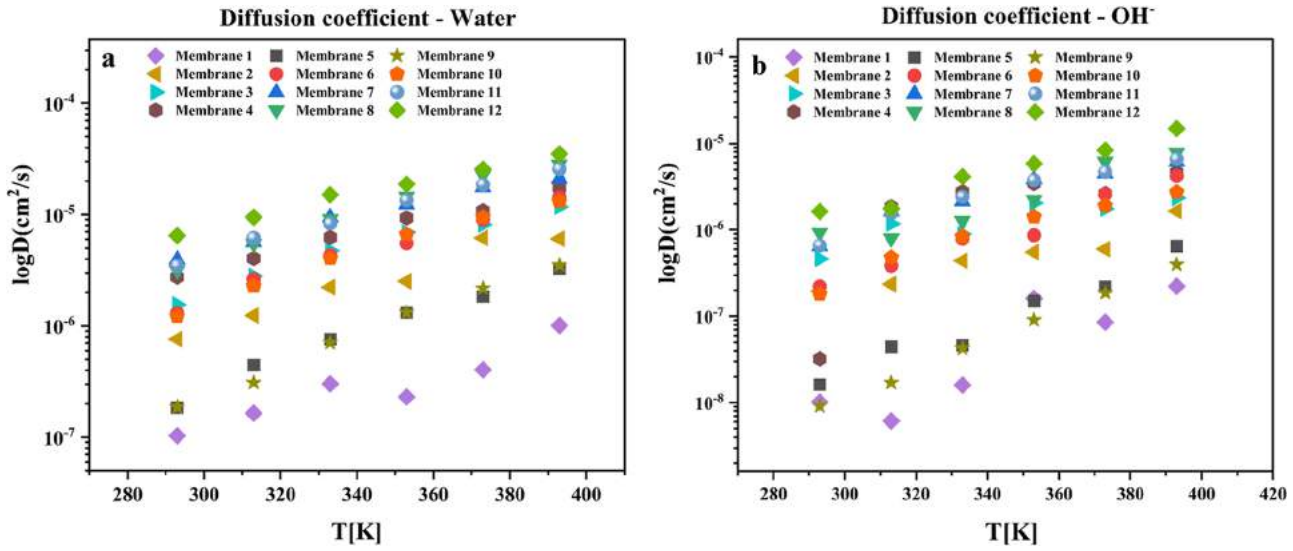

Figure 5. Diffusion coefficients log(D) computed at different temperatures for (a) water molecules and (b) hydroxide anion (refer to Table 1 for membranes specifications).

structures were initially cooled at 0.3 K with the *NVT* ensemble for 2.5 ns, using the pcff+ force field. Then, the force field was switched to ReaxFF and the cells were heated to 293 K with 500 ps of *NVT* followed by 1 ns of *NPT* at 1 atm.

The density and RDF were compared to those obtained with pcff+. The resulting density (~1.17 g/cm^3) is slightly higher than that obtained with pcff+, but still in good agreement with the experimental values. The increase in density is due to the stronger interaction arising among the atoms, as confirmed by the RDF results (Figure S5). This is demonstrated by peaks of N−O and N−N $g(r)$ at smaller distances compared to pcff+, proving that a stronger interaction is arising between charged groups.

Potential Mean Force. The PMF (kJ/mol) profiles are shown as functions of the N−O distance r (Å) in Figure 4a,b. The minimum PMF values for each structure are shown in Figure 4c and the corresponding values are reported in Table S3. The lower the depth of the well in the PMF profile, the weaker the electrostatic interaction between the cationic group and anionic species. As the water content increases, the interaction becomes weaker. This implies that the hydroxide can more easily dissociate from the functional group, and better conductivity is expected. An increase in the level of amination leads to reduced electrostatic interaction, but this behavior is presumably connected to the higher water uptake favored by the presence of more functional groups. A much stronger interaction is observed in membranes with 10% amination, while no significant difference was discerned between 30 and 50% amination.

Vehicular Diffusion Coefficient. The vehicular diffusion coefficients of both water molecules (D_W) and OH^- ions (D_{OH}) were calculated via the MSD route. The MSDs were derived from 10 ns *NVT* runs for all membranes at various temperatures, ranging from 293 to 393 K, with temperature steps of 20 K. The dynamic analysis was anticipated by alternating *NVT* and *NPT* ensembles to gradually reach the desired T and stabilize the structure.

The MSD curves of water molecules (a) and hydroxide anions (b) for membrane 3 at variable temperatures are displayed in Figure S6. The diffusion coefficients were obtained from the long-time region slope of the MSD curve, as short-time regions characterize a subdiffusion behavior where hydroxide anions are simply rattling among water molecules.[49]

https://doi.org/10.1021/acs.jpcc.3c07118
J. Phys. Chem. C 2024, 128, 623−634

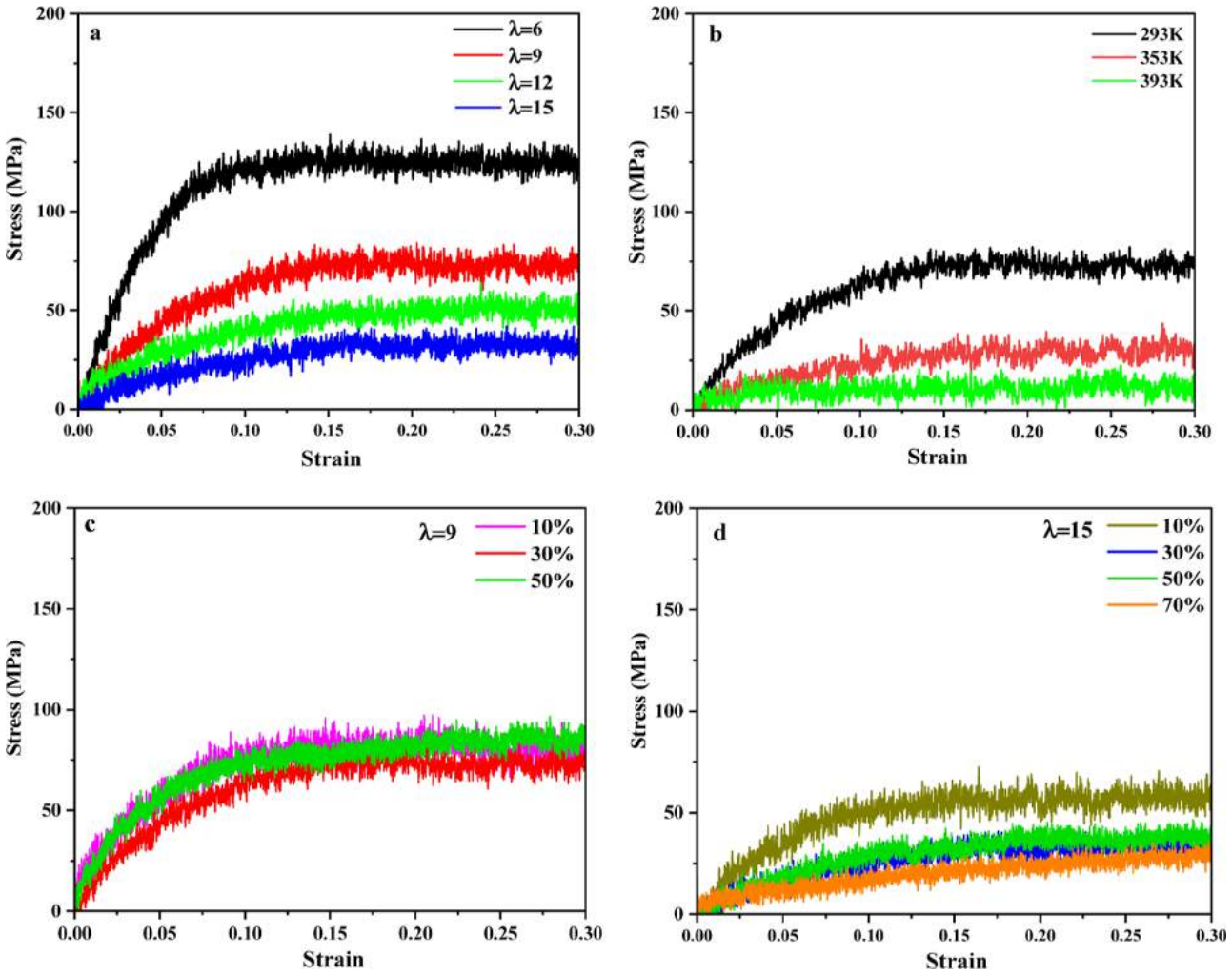

Figure 6. Stress−strain curves as a function of (a) hydration level, (b) temperature, and (c,d) degree of amination at λ = 9 and 15, respectively.

The diffusion coefficients were subsequently calculated using the simple Einstein's relation. The obtained results are shown in Figure 5 and reported in Table S4 (at 293 and 393 K).

As expected, D_{OH} is lower than D_W, due to the electrostatic interaction of the anions with the cationic groups and the stronger solvation structure. Moreover, an increase in the temperature and hydration level is responsible for a relevant increase in diffusivity. This becomes more significant when approaching water bulk conditions. On the contrary, at lower water contents the tortuous structure of the hydrophilic channels, or the isolated clusters, is blocking vehicular diffusion. Overall λ has a greater impact than the degree of amination. In fact, comparing membrane 11 (50% amination and 3300 H_2O molecules) with membrane 8 (30% amination and 2520 H_2O molecules), the latter demonstrated higher diffusivity (7.82×10^{-7} cm^2/s, compared to 6.63×10^{-7} cm^2/s, at 393 K). In the first case, the water−QA electrostatic interaction is stronger, as suggested by the PMF analysis, and the vehicular diffusion is slowed down. The PMF curves for the two systems are displayed in Figure S7. On the other side, a slight decrease of D_{OH} is observed at higher amination and lower λ (comparing membranes 5 and 6 with membranes 9 and 10, respectively) (Table S4). In these cases, the electrostatic interaction is stronger for membranes with 30% amination (Table S3). Therefore, the trend of diffusivity may be ascribed to the lower mobility of polymer chain since more pyrrolic rings are introduced into the backbone.[22] The higher diffusion coefficient at larger water content (membrane 12) can be attributed to a more developed hydrophilic network, which contrasts the effect of lower mobility. With 10% amination, the diffusion is lower, and accordingly, a higher degree of functionalization is required to grant a higher ionic conductivity.

Despite the absence of the Grotthuss mechanism in the simulation with pcff+, which should provide a consistent contribution to overall conductivity, the general trend of the OH^- diffusion coefficient is not expected to change dramatically as a function of level of hydration, amination, and temperature.

Different studies[64,68,69] proved that both OH^- and H_2O diffusion become faster as temperature increases, due to a reduction of the activation energy associated with ion hopping. Water content plays an important role, and in particular the nanophase segregation between hydrophobic and hydrophilic regions. Even though Grotthuss mechanism enables a faster transport of hydroxide species through narrow bottlenecks in water channels,[35,70] both theoretical and experimental studies proved that the overall conductivity increases with growing λ and in the presence of well-defined water channels.[36,53,58,71,72] The increase in amination degree and IEC is generally expected to improve the ionic conductivity.[31,73,74] For PA membranes, however, a growth in IEC is associated with a

https://doi.org/10.1021/acs.jpcc.3c07118
J. Phys. Chem. C 2024, 128, 623−634

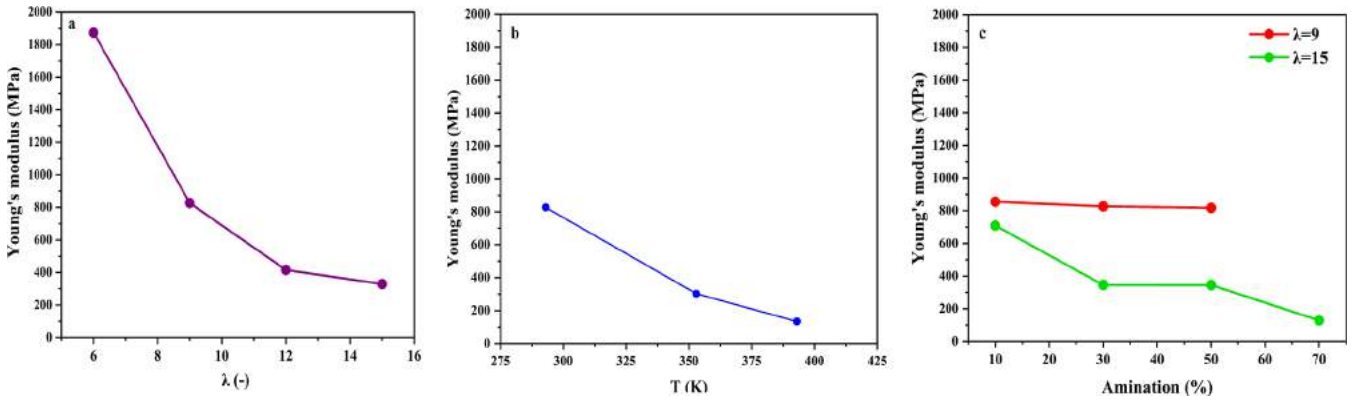

Figure 7. Young's modulus (MPa) as a function of (a) hydration level λ, (b) temperature, and (c) degree of amination with λ = 9 and λ = 12.

reduced chain mobility due to the introduction of N-substituted pyrrole units, which in turn reduces the ionic conductivity above certain values of IEC and at relatively low λ. The experimental findings by Zhou et al.[21,22] are in accordance with our simulations. As a result, no major variation in the trend of diffusivity is expected due to the exclusion of the Grotthuss mechanism.

To conclude, the anomalous diffusion exponents (n) were computed from the slope of the log−log MSD plot at long-time regions (Figure S8), to quantify the deviation from normal diffusion. At high λ and amination degrees, the values approach unity ($0.8 < n < 1$), and we can assume the results obtained with simple Einstein's relation to be correct. Instead, at lower levels of hydration and amination the value of n is far from unity, suggesting a deviation from normal diffusion. In this respect, the modified Einstein's relation should be used, which in turn would provide lower values of diffusion coefficient.

Mechanical Analysis. Despite the discernible benefit in terms of diffusivity, excessive water uptake could cause an overswelling of the membrane and irreversible plastic deformation.[31] Mechanical analysis was performed to assess whether the improved conductivity would be offset by a worsening of the mechanical properties of the membrane.

The obtained stress−strain curves are shown in Figure 6. Only the elastic region has been investigated in this study, which is sufficient for a first qualitative analysis.[75] The intention of this work is to analyze the dependency of Young's modulus on the different parameters, which is depicted in Figure 7, and the numerical values of the computed moduli are reported in Table S5.

Figure 6a shows the influence of the hydration level (λ = 6, 9, 12, 15) on the mechanical properties of the membranes with 30% amination and at constant T = 293 K. The water inside the hydrophilic channels has a softening effect. Accordingly, both the Young's modulus and the yield stress decrease. The effect of water content is much stronger between λ = 6 and 9, whereas it is attenuated at higher hydration levels (Figure 7a). Figure 6b shows the effect of temperature on membrane 7, at 293, 353, and 393 K. Temperature also has a softening effect, but lower compared to that of λ. The obtained results are consistent with the data available in the literature and with experimental observations.[30,33,61,75]

Figure 6c,d outline the effect of amination's degree on the mechanical properties, at constant room temperature and λ equal to 9 and 15, respectively. An increased number of QA groups was expected to significantly deteriorate the membrane's mechanical properties due to the higher water uptake. However, the effect of amination is minor despite the large difference in water content. For instance, the decrease in Young's modulus is considerably greater between membrane 6 and membrane 8 than between membrane 6 and membrane 10, even though membrane 10 contains more water molecules (Figure 7a,c). This behavior can be attributed to the presence of the pyrrolic rings in the polymer backbone (Scheme 1) that balance the softening effect of water. Additionally, the presence of hydrogen bonding between the functional groups may enhance the membrane's mechanical stability.[25]

The Young's modulus at λ = 15 is shown in Figure 7c. A new membrane (membrane 13) with 70% amination has been simulated, with further details provided in Table S6. In this case, the excessive softening of the membrane is not balanced by a significant increase in diffusivity. Membranes with 30 and 50% of amination show, instead, comparable values of Young's modulus. Therefore, it can be concluded that 30−50% of amination is a reasonable compromise between good mechanical properties and enhanced ionic conductivity.

CONCLUSIONS

In the present article, all-atom MD simulations were carried out to investigate both static and dynamic properties of hydrated PA-AEMs. The structural, diffusion, and mechanical properties were explored as a function of the level of hydration λ, the degree of amination of the polymer, and the temperature. The static analysis confirmed the formation of interconnected hydrophilic channels as the water content and amination of the membrane increased, creating a continuous pathway for ionic transport. However, at a lower degree of amination (10%), this condition was attained only at the highest λ, indicating that higher levels of amination are necessary to ensure ionic transport.

Dynamic simulations showed that the diffusion coefficients and the mechanical stability of hydrated membranes manifest opposite behavior as a function of the water content, temperature, and polymer chemistry. A suitable compromise between the enhanced conductivity and good mechanical properties must be reached. At 10% amination, the diffusion was too low, and 70% amination caused an excessive deterioration of the mechanical properties. Therefore, we can reasonably conclude that a good compromise can be found with 30% amination, which allows for an optimal balance of diffusivity and mechanical stability, with a reduced reaction time.

https://doi.org/10.1021/acs.jpcc.3c07118
J. Phys. Chem. C 2024, 128, 623−634

■ ASSOCIATED CONTENT

Supporting Information

The Supporting Information is available free of charge at https://pubs.acs.org/doi/10.1021/acs.jpcc.3c07118.

Additional geometric information on simulated structures; size effect analysis; densities; RDF and CN of different membranes; comparison of pcff+ and ReaxFF RDF with DFT analysis; RDF with ReaxFF; minimum values of PMFs; diffusion coefficients of water and hydroxide anions; anomalous diffusion exponents; and elastic moduli as a function of hydration level, temperature, and degree of amination (PDF)

pcff + parameters (PDF)

■ AUTHOR INFORMATION

Corresponding Author

Narges Ataollahi − *Department of Civil, Environmental and Mechanical Engineering, University of Trento, Trento 38123, Italy;* orcid.org/0000-0002-8135-6054; Email: narges.ataollahi@unitn.it

Authors

Eleonora Tomasino − *Department of Civil, Environmental and Mechanical Engineering, University of Trento, Trento 38123, Italy;* orcid.org/0000-0002-4090-5774

Binayak Mukherjee − *Department of Civil, Environmental and Mechanical Engineering, University of Trento, Trento 38123, Italy;* Present Address: Materials Research and Technology Department, Luxembourg Institute of Science and Technology (LIST), Av. des Hauts-Fourneaux 5, L-4362 Esch-sur-Alzette, Luxembourg

Varun Donnakatte Neelalochana − *Department of Civil, Environmental and Mechanical Engineering, University of Trento, Trento 38123, Italy;* orcid.org/0000-0002-2433-1889

Paolo Scardi − *Department of Civil, Environmental and Mechanical Engineering, University of Trento, Trento 38123, Italy;* orcid.org/0000-0003-1097-3917

Complete contact information is available at: https://pubs.acs.org/10.1021/acs.jpcc.3c07118

Author Contributions

The manuscript was written through contributions of all authors. All authors have given approval to the final version of the manuscript.

Notes

The authors declare no competing financial interest.

■ ACKNOWLEDGMENTS

This research was partially funded through the strategic project "Modelling & Simulation" of the University of Trento. The authors are thankful to Dr. Himanshu Nautiyal, and to David Reith, from the staff of MedeA, for the technical support, and to Prof. Luca Deseri for the useful suggestions. The authors also acknowledge the Italian Ministry of Universities and Research (MUR), in the framework of the project DICAM-EXC (Departments of Excellence 2023-2027, grant L232/2016).

■ REFERENCES

(1) Ataollahi, N.; Vezzù, K.; Nawn, G.; Pace, G.; Cavinato, G.; Girardi, F.; Scardi, P.; Di Noto, V.; Di Maggio, R. A Polyketone-Based Anion Exchange Membrane for Electrochemical Applications: Synthesis and Characterization. *Electrochim. Acta* **2017**, *226*, 148−157.

(2) Chen, D.; Hickner, M. A.; Agar, E.; Kumbur, E. C. Optimized Anion Exchange Membranes for Vanadium Redox Flow Batteries. *ACS Appl. Mater. Interfaces* **2013**, *5* (15), 7559−7566.

(3) Alvi, A. R.; Vezzù, K.; Pagot, G.; Sgarbossa, P.; Pace, G.; Di Noto, V. Inorganic-Organic Hybrid Anion Conducting Membranes Based on Ammonium-Functionalized Polyethylene Pyrrole-Polyethylene Ketone Copolymer. *Macromol. Chem. Phys.* **2022**, *223* (8), 2100409.

(4) Santoro, C.; Lavacchi, A.; Mustarelli, P.; Di Noto, V.; Elbaz, L.; Dekel, D. R.; Jaouen, F. What Is Next in Anion-Exchange Membrane Water Electrolyzers? Bottlenecks, Benefits, and Future. *ChemSusChem* **2022**, *15* (8), No. e202200027.

(5) Hwang, S. Y.; Kim, J. J.; Park, E. J.; Hwang, T. S. Synthesis of Polyketone Anion Ion Exchange Fibers by Paal-Knorr Reaction and Its Physico-Chemical Properties. *Macromol. Res.* **2020**, *28* (5), 465−471.

(6) Pal, S.; Mondal, R.; Chandel, A. K. S.; Chatterjee, U. Composite Anion Exchange Membranes with Antibacterial Properties for Desalination and Fluoride Ion Removal. *ACS EST Water* **2021**, *1* (10), 2206−2216.

(7) Khan, M. I.; Luque, R.; Akhtar, S.; Shaheen, A.; Mehmood, A.; Idress, S.; Buzdar, S. A.; ur Rehman, A. Design of Anion Exchange Membranes and Electrodialysis Studies for Water Desalination. *Materials* **2016**, *9* (5), 365.

(8) Das, G.; Choi, J. H.; Nguyen, P. K. T.; Kim, D. J.; Yoon, Y. S. Anion Exchange Membranes for Fuel Cell Application: A Review. *Polymers* **2022**, *14* (6), 1197.

(9) Dekel, D. R. Review of Cell Performance in Anion Exchange Membrane Fuel Cells. *J. Power Sources* **2018**, *375*, 158−169.

(10) Rezayani, M.; Sharif, F.; Makki, H. Understanding Ion Diffusion in Anion Exchange Membranes; Effects of Morphology and Mobility of Pendant Cationic Groups. *J. Mater. Chem. A* **2022**, *10*, 18295−18307.

(11) Zhang, Y.; Fang, J.; Wu, Y.; Xu, H.; Chi, X.; Li, W.; Yang, Y.; Yan, G.; Zhuang, Y. Novel Fluoropolymer Anion Exchange Membranes for Alkaline Direct Methanol Fuel Cells. *J. Colloid Interface Sci.* **2012**, *381*, 59−66.

(12) Takaba, H.; Shimizu, N.; Hisabe, T.; Alam, M. K. Modeling of Transport Mechanisms of OH- in Electrolyte of Alkaline Fuel Cell. *ECS Trans.* **2014**, *61* (13), 63−69.

(13) Fang, J.; Qiao, J.; Wilkinson, D. P.; Zhang, J. *Electrochemical Polymer Electrolyte Membranes*, 1st ed.; CRC Press: Boca Raton, 2015.

(14) Pan, Z. F.; Chen, R.; An, L.; Li, Y. S. Alkaline Anion Exchange Membrane Fuel Cells for Cogeneration of Electricity and Valuable Chemicals. *J. Power Sources* **2017**, *365*, 430−445.

(15) Ran, J.; Wu, L.; He, Y.; Yang, Z.; Wang, Y.; Jiang, C.; Ge, L.; Bakangura, E.; Xu, T. Ion Exchange Membranes: New Developments and Applications. *J. Membr. Sci.* **2017**, *522*, 267−291.

(16) Varcoe, J. R.; Atanassov, P.; Dekel, D. R.; Herring, A. M.; Hickner, M. A.; Kohl, P. A.; Kucernak, A. R.; Mustain, W. E.; Nijmeijer, K.; Scott, K.; Xu, T.; Zhuang, L. Anion-Exchange Membranes in Electrochemical Energy Systems. *Energy Environ. Sci.* **2014**, *7*, 3135−3191.

(17) Hagesteijn, K. F. L.; Jiang, S.; Ladewig, B. P. A Review of the Synthesis and Characterization of Anion Exchange Membranes. *J. Mater. Sci.* **2018**, *53* (16), 11131−11150.

(18) Gottesfeld, S.; Dekel, D. R.; Page, M.; Bae, C.; Yan, Y.; Zelenay, P.; Kim, Y. S. Anion Exchange Membrane Fuel Cells: Current Status and Remaining Challenges. *J. Power Sources* **2018**, *375*, 170−184.

(19) Donnakatte Neelalochana, V.; Tomasino, E.; Di Maggio, R.; Cotini, O.; Scardi, P.; Mammi, S.; Ataollahi, N. Anion Exchange Membranes Based on Chemical Modification of Recycled PET Bottles. *ACS Appl. Polym. Mater.* **2023**, *5* (9), 7548−7561.

(20) Zhou, Y. C.; Zhang, Z. M.; Zhou, L.; Bao, R. Y.; Liu, Z. Y.; Yang, M. B.; Yang, W. Imidazole-Functionalized Polyketone-Based Polyelectrolytes with Efficient Ionic Channels and Superwettability

for Alkaline Polyelectrolyte Fuel Cells and Multiple Liquid Purification. *J. Mater. Chem. A* **2021**, *9* (26), 14827−14840.
(21) Zhou, Y. C.; Bao, R. Y.; Liu, Z.; Yang, M. B.; Yang, W. Electrospun Modified Polyketone-Based Anion Exchange Membranes with High Ionic Conductivity and Robust Mechanical Properties. *ACS Appl. Energy Mater.* **2021**, *4* (5), 5187−5200.
(22) Zhou, Y. C.; Zhou, L.; Feng, C. P.; Wu, X. T.; Bao, R. Y.; Liu, Z. Y.; Yang, M. B.; Yang, W. Direct Modification of Polyketone Resin for Anion Exchange Membrane of Alkaline Fuel Cells. *J. Colloid Interface Sci.* **2019**, *556*, 420−431.
(23) Nawn, G.; Vezzù, K.; Cavinato, G.; Pace, G.; Bertasi, F.; Pagot, G.; Negro, E.; Di Noto, V. Opening Doors to Future Electrochemical Energy Devices: The Anion-Conducting Polyketone Polyelectrolytes. *Adv. Funct. Mater.* **2018**, *28* (29), 1706522.
(24) Ataollahi, N.; Girardi, F.; Cappelletto, E.; Vezzù, K.; Di Noto, V.; Scardi, P.; Callone, E.; Di Maggio, R. Chemical Modification and Structural Rearrangements of Polyketone-Based Polymer Membrane. *J. Appl. Polym. Sci.* **2017**, *134*, 45485.
(25) Ataollahi, N.; Tomasino, E.; Cotini, O.; Di Maggio, R. Enhanced OH- Conductivity for Fuel Cells with Anion Exchange Membranes, Based on Modified Terpolymer Polyketone and Surface Functionalized Silica. *Energies* **2022**, *15* (5), 1953.
(26) Ataollahi, N.; Cappelletto, E.; Vezzù, K.; di Noto, V.; Cavinato, G.; Callone, E.; Dirè, S.; Scardi, P.; di Maggio, R. Properties of Anion Exchange Membrane Based on Polyamine: Effect of Functionalized Silica Particles Prepared by Sol-Gel Method. *Solid State Ionics* **2018**, *322*, 85−92.
(27) Cui, R.; Li, S.; Yu, C.; Wang, Y.; Zhou, Y. Understanding the Mechanism of Nitrogen Transport in the Perfluorinated Sulfonic-Acid Hydrated Membranes via Molecular Dynamics Simulations. *J. Membr. Sci.* **2022**, *648*, 120328.
(28) Sengupta, S.; Lyulin, A. V. Molecular Modeling of Structure and Dynamics of Nafion Protonation States. *J. Phys. Chem. B* **2019**, *123* (31), 6882−6891.
(29) Rezayani, M.; Sharif, F.; Netz, R. R.; Makki, H. Insight into the Relationship between Molecular Morphology and Water/Ion Diffusion in Cation Exchange Membranes: Case of Partially Sulfonated Polyether Sulfone. *J. Membr. Sci.* **2022**, *654*, 120561.
(30) Kuo, A. T.; Shinoda, W.; Okazaki, S. Molecular Dynamics Study of the Morphology of Hydrated Perfluorosulfonic Acid Polymer Membranes. *J. Phys. Chem. C* **2016**, *120* (45), 25832−25842.
(31) Di Salvo, J. L.; De Luca, G.; Cipollina, A.; Micale, G. Effect of Ion Exchange Capacity and Water Uptake on Hydroxide Transport in PSU-TMA Membranes: A DFT and Molecular Dynamics Study. *J. Membr. Sci.* **2020**, *599*, 117837.
(32) Zhang, K.; Yu, W. S.; Ge, X.; Wu, L.; Xu, T. Molecular Dynamics Insight into Phase Separation and Transport in Anion-Exchange Membranes: Effect of Hydrophobicity of Backbones. *J. Membr. Sci.* **2022**, *661*, 120922.
(33) Feng, C.; Li, Y.; Qu, K.; Zhang, Z.; He, P. Mechanical Behavior of a Hydrated Perfluorosulfonic Acid Membrane at Meso and Nano Scales. *RSC Adv.* **2019**, *9* (17), 9594−9603.
(34) Dong, D.; Zhang, W.; Van Duin, A. C. T.; Bedrov, D. Grotthuss versus Vehicular Transport of Hydroxide in Anion-Exchange Membranes: Insight from Combined Reactive and Nonreactive Molecular Simulations. *J. Phys. Chem. Lett.* **2018**, *9* (4), 825−829.
(35) Dong, D.; Wei, X.; Hooper, J. B.; Pan, H.; Bedrov, D. Role of Cationic Groups on Structural and Dynamical Correlations in Hydrated Quaternary Ammonium-Functionalized Poly(p-Phenylene Oxide)-Based Anion Exchange Membranes. *Phys. Chem. Chem. Phys.* **2018**, *20* (29), 19350−19362.
(36) Zhang, W.; Dong, D.; Bedrov, D.; Van Duin, A. C. T. Hydroxide Transport and Chemical Degradation in Anion Exchange Membranes: A Combined Reactive and Non-Reactive Molecular Simulation Study. *J. Mater. Chem. A* **2019**, *7* (10), 5442−5452.
(37) Tomasino, E.; Mukherjee, B.; Ataollahi, N.; Scardi, P. Water Uptake in an Anion Exchange Membrane Based on Polyamine: A First-Principles Study. *J. Phys. Chem. B* **2022**, *126* (38), 7418−7428.
(38) *MedeA*, version 3.0; Materials Design Inc.: San Diego, USA, 2019. https://www.materialsdesign.com/medea-software.
(39) Bahlakeh, G.; Nikazar, M. Molecular Dynamics Simulation Analysis of Hydration Effects on Microstructure and Transport Dynamics in Sulfonated Poly(2,6-Dimethyl-1,4- Phenylene Oxide) Fuel Cell Membranes. *Int. J. Hydrogen Energy* **2012**, *37* (17), 12714−12724.
(40) Plimpton, S. Fast Parallel Algorithms for Short-Range Molecular Dynamics. *J. Comput. Phys.* **1995**, *117* (1), 1−19.
(41) Sun, H.; Mumby, S. J.; Maple, J. R.; Hagler', A. T. An Ab Initio CFF93 All-Atom Force Field for Polycarbonates. *J. Am. Chem. SOC* **1994**, *116*, 2978−2987.
(42) Bonthuis, D. J.; Mamatkulov, S. I.; Netz, R. R. Optimization of Classical Nonpolarizable Force Fields for OH− and H3O+. *J. Chem. Phys.* **2016**, *144* (10), 104503.
(43) Swope, W. C.; Andersen, H. C.; Berens, P. H.; Wilson, K. R. A Computer Simulation Method for the Calculation of Equilibrium Constants for the Formation of Physical Clusters of Molecules: Application to Small Water Clusters. *J. Chem. Phys.* **1982**, *76* (1), 637−649.
(44) Hockney, R. W.; Eastwood, J. W. *Computer Simulation Using Particles*; CRC Press, 1988.
(45) Warshel, A.; Lifson, S. Consistent Force Field Calculations. II. Crystal Structures, Sublimation Energies, Molecular and Lattice Vibrations, Molecular Conformations, and Enthalpies of Alkanes. *J. Chem. Phys.* **1970**, *53* (2), 582−594.
(46) Nosé, S. A Unified Formulation of the Constant Temperature Molecular Dynamics Methods. *J. Chem. Phys.* **1984**, *81* (1), 511−519.
(47) Brunello, G. F.; Mateker, W. R.; Lee, S. G.; Choi, J., II; Jang, S. S. Effect of Temperature on Structure and Water Transport of Hydrated Sulfonated Poly(Ether Ether Ketone): A Molecular Dynamics Simulation Approach. *Journal of Renewable and Sustainable Energy* **2011**, *3* (4), 043111.
(48) Zhang, W.; Van Duin, A. C. T. Second-Generation ReaxFF Water Force Field: Improvements in the Description of Water Density and OH-Anion Diffusion. *J. Phys. Chem. B* **2017**, *121* (24), 6021−6032.
(49) Dubey, V.; Maiti, A.; Daschakraborty, S. Predicting the Solvation Structure and Vehicular Diffusion of Hydroxide Ion in an Anion Exchange Membrane Using Nonreactive Molecular Dynamics Simulation. *Chem. Phys. Lett.* **2020**, *755*, 137802.
(50) Zelovich, T.; Tuckerman, M. E. OH− and H3O + Diffusion in Model AEMs and PEMs at Low Hydration: Insights from Ab Initio Molecular Dynamics. *Membranes* **2021**, *11* (5), 355.
(51) Tuckerman, M. E.; Marx, D.; Parrinello, M. The Nature and Transport Mechanism of Hydrated Hydroxide Ions in Aqueous Solution. *Nature* **2002**, *417* (6892), 925−929.
(52) Zelovich, T.; Long, Z.; Hickner, M.; Paddison, S. J.; Bae, C.; Tuckerman, M. E. Ab Initio Molecular Dynamics Study of Hydroxide Diffusion Mechanisms in Nanoconfined Structural Mimics of Anion Exchange Membranes. *J. Phys. Chem. C* **2019**, *123* (8), 4638−4653.
(53) Zelovich, T.; Vogt-Maranto, L.; Hickner, M. A.; Paddison, S. J.; Bae, C.; Dekel, D. R.; Tuckerman, M. E. Hydroxide Ion Diffusion in Anion-Exchange Membranes at Low Hydration: Insights from Ab Initio Molecular Dynamics. *Chem. Mater.* **2019**, *31* (15), 5778−5787.
(54) Pusara, S.; Srebnik, S.; Dekel, D. R. Molecular Simulation of Quaternary Ammonium Solutions at Low Hydration Levels. *J. Phys. Chem. C* **2018**, *122* (21), 11204−11213.
(55) Amel, A.; Gavish, N.; Zhu, L.; Dekel, D. R.; Hickner, M. A.; Ein-Eli, Y. Bicarbonate and Chloride Anion Transport in Anion Exchange Membranes. *J. Membr. Sci.* **2016**, *514*, 125−134.
(56) Zhu, Z.; Tuckerman, M. E. Ab Initio Molecular Dynamics Investigation of the Concentration Dependence of Charged Defect Transport in Basic Solutions via Calculation of the Infrared Spectrum. *J. Phys. Chem. B* **2002**, *106* (33), 8009−8018.
(57) Dong, D.; Zhang, W.; Barnett, A.; Lu, J.; van Duin, A. C. T.; Molinero, V.; Bedrov, D. Multiscale Modeling of Structure, Transport and Reactivity in Alkaline Fuel Cell Membranes: Combined Coarse-

https://doi.org/10.1021/acs.jpcc.3c07118
J. Phys. Chem. C 2024, 128, 623−634

Grained, Atomistic and Reactive Molecular Dynamics Simulations. *Polymers* **2018**, *10* (11), 1289.
(58) Zhang, W.; Van Duin, A. C. T. ReaxFF Reactive Molecular Dynamics Simulation of Functionalized Poly(Phenylene Oxide) Anion Exchange Membrane. *J. Phys. Chem. C* **2015**, *119* (49), 27727−27736.
(59) Merinov, B. V.; Goddard, W. A. Computational Modeling of Structure and OH-Anion Diffusion in Quaternary Ammonium Polysulfone Hydroxide - Polymer Electrolyte for Application in Electrochemical Devices. *J. Membr. Sci.* **2013**, *431*, 79−85.
(60) Berrod, Q.; Hanot, S.; Guillermo, A.; Mossa, S.; Lyonnard, S. Water Sub-Diffusion in Membranes for Fuel Cells. *Sci. Rep.* **2017**, *7* (1), 8326.
(61) Vandiver, M. A.; Caire, B. R.; Carver, J. R.; Waldrop, K.; Hibbs, M. R.; Varcoe, J. R.; Herring, A. M.; Liberatore, M. W. Mechanical Characterization of Anion Exchange Membranes by Extensional Rheology under Controlled Hydration. *J. Electrochem. Soc.* **2014**, *161* (10), H677−H683.
(62) Kundu, S.; Simon, L. C.; Fowler, M.; Grot, S. Mechanical Properties of Nafion^{TM} Electrolyte Membranes under Hydrated Conditions. *Polymer* **2005**, *46* (25), 11707−11715.
(63) Chen, W.; Wu, X.; Li, T.; Yan, X.; Zhang, Y.; Wang, X.; Zhang, F.; Zhang, S.; He, G. Structural Contribution of Cationic Groups to Water Sorption in Anion Exchange Membranes: A Combined DFT and MD Simulation Study. *Chem. Eng. Sci.* **2021**, *244*, 116791.
(64) Chen, C.; Tse, Y. L. S.; Lindberg, G. E.; Knight, C.; Voth, G. A. Hydroxide Solvation and Transport in Anion Exchange Membranes. *J. Am. Chem. Soc.* **2016**, *138* (3), 991−1000.
(65) Neese, F. The ORCA Program System. *WIREs Comput. Mol. Sci.* **2012**, *2*, 73−78.
(66) Caldeweyher, E.; Bannwarth, C.; Grimme, S. Extension of the D3 Dispersion Coefficient Model. *J. Chem. Phys.* **2017**, *147* (3), 034112.
(67) Pisani, W. A.; Radue, M. S.; Chinkanjanarot, S.; Bednarcyk, B. A.; Pineda, E. J.; Waters, K.; Pandey, R.; King, J. A.; Odegard, G. M. Multiscale Modeling of PEEK Using Reactive Molecular Dynamics Modeling and Micromechanics. *Polymer* **2019**, *163*, 96−105.
(68) Zhang, G.; Yang, G.; Li, S.; Shen, Q.; Wang, H.; Li, Z.; Zhou, Y.; Ye, W. Effects of Hydration and Temperature on the Microstructure and Transport Properties of Nafion Polyelectrolyte Membrane: A Molecular Dynamics Simulation. *Membranes* **2021**, *11* (9), 695.
(69) Ma, Z.; Tuckerman, M. E. On the Connection between Proton Transport, Structural Diffusion, and Reorientation of the Hydrated Hydroxide Ion as a Function of Temperature. *Chem. Phys. Lett.* **2011**, *511* (4−6), 177−182.
(70) Ramírez, S. C.; Paz, R. R. Hydroxide Transport in Anion-Exchange Membranes for Alkaline Fuel Cells. In *New Trends in Ion Exchange Studies*; Karakuş, S., Ed.; InTech, 2018.
(71) Li, N.; Guiver, M. D.; Binder, W. H. Towards High Conductivity in Anion-Exchange Membranes for Alkaline Fuel Cells. *ChemSusChem* **2013**, *6* (8), 1376−1383.
(72) Rezayani, M.; Sharif, F.; Makki, H. Understanding Ion Diffusion in Anion Exchange Membranes; Effects of Morphology and Mobility of Pendant Cationic Groups. *J. Mater. Chem. A* **2022**, *10* (35), 18295−18307.
(73) Sireci, E.; De Luca, G.; Luque Di Salvo, J.; Cipollina, A.; Micale, G. Prediction of Equilibrium Water Uptake and Ions Diffusivities in Ion-Exchange Membranes Combining Molecular Dynamics and Analytical Models. *J. Membr. Sci.* **2023**, *668*, 121283.
(74) Abouzari-Lotf, E.; Jacob, M. V.; Ghassemi, H.; Zakeri, M.; Nasef, M. M.; Abdolahi, Y.; Abbasi, A.; Ahmad, A. Highly Conductive Anion Exchange Membranes Based on Polymer Networks Containing Imidazolium Functionalised Side Chains. *Sci. Rep.* **2021**, *11* (1), 3764.
(75) Kuo, A. T.; Takeuchi, K.; Tanaka, A.; Urata, S.; Okazaki, S.; Shinoda, W. Exploring the Effect of Pendent Side Chain Length on the Structural and Mechanical Properties of Hydrated Perfluorosulfonic Acid Polymer Membranes by Molecular Dynamics Simulation. *Polymer* **2018**, *146*, 53−62.

https://doi.org/10.1021/acs.jpcc.3c07118
J. Phys. Chem. C 2024, 128, 623−634